

HEAT TRANSFER AND EVAPORATION OF SALT SOLUTION ON A HORIZONTAL HEATING WALL

by

Sergey Y. MISYURA

Kutateladze Institute of Thermophysics Siberian Branch, Russian Academy of Sciences,
Novosibirsk, Russia

Original scientific paper
<https://doi.org/10.2298/TSCI180521281M>

An experimental study of non-isothermal heat transfer and evaporation of thin layers of aqueous solutions of salts has been carried out. Evaporation was realized on a horizontal heated wall in the air atmosphere at a pressure of 1 bar. In the evaporation of water and salt solution, the heat transfer coefficient is constant for a long time period and increases in the final stage due to the multiple reduction of the layer thickness. Evaporation curves for different types of salt solutions have a different character. Due to the increase in salt concentration, the evaporation rate of LiBr-water, CaCl₂-water, LiCl-water, and MgCl₂-water decreases over time. Salt solutions decreases with time. Evaporation rates for solutions of NaCl-water, CsCl-water, and BaCl₂-water slightly change over time. To analyze the effect of free convection on heat transfer, experimental curves for the ratio of Nusselt numbers ($A = Nu_{(salt)}/Nu_{(water)}$) for the salt and water solution have been built. Parameter A is greater than one and increases with time. The effect of convection on heat transfer varies with time and depends on the current salt concentration and solution layer height, which should be considered in the simulation.

Key words: layer heat transfer, salt solution, evaporation rate

Introduction

Evaporation of aqueous salt solutions is widely observed in natural conditions and is used in technical devices. The aqueous salt solutions CaCl₂-water, LiBr-water, and LiCl-water are used in energy, in absorption heat pumps [1] to produce heat and cold. This technology is based on physical principles based on the use of heat of evaporation and absorption. In many chemical technologies at high heat fluxes, physical, physical properties of salt solutions and thermodynamic equilibrium curves change significantly during non-isothermal evaporation [2]. High temperature evaporation of aqueous salt solutions is used in desalination and chemical technologies [2]. In the presence of an intense heat flux on the wall, the falling film of the solution tends to thicken locally and to rupture [3], which leads to a sharp drop in the absorption efficiency in the heat pump absorber and a decrease in the evaporation rate in the high temperature generator. Calculation of heat and mass transfer in the salt solution film is given in [4, 5].

The instability of film is driven by disjoining pressure [6]. The behavior of free convection in a film was described in [7, 8]. Heat and mass transfer during evaporation of a thin layer was discussed in [9-12]. Changes in the heat transfer coefficient for a falling film of solution were considered in [13]. In most numerical studies, prediction of the heat transfer coeffi-

cient in a liquid film does not take into account the free convection in an aqueous salt solution [14-16]. The neglect of convection in the simulation of high temperature evaporation leads to a significant underestimation of the evaporation rate of the salt solution [17]. With increasing time, the salt concentration increases, and the evaporation rate falls several times [18, 19].

In the vicinity of the evaporating layer and droplets, a vapor-gas layer is formed and it reduces the evaporation rate and affects free convection in the gas [20-22]. Bubble boiling in water-salt solution drastically increases the evaporation rate and heat exchange [18]. Currently, structured surfaces are widely used to enhance heat and mass transfer [23, 24].

For all salt solutions, which are discussed in this article, the physical properties change significantly with increasing salt concentration. Equilibrium curves and physical properties of salt solutions in a wide range of salt concentrations are presented in [25-27]. Experimental investigations of a hydrophobic membrane with aqueous solution of LiBr salt were discussed in [28].

Evaporation of highly concentrated salt solutions leads to the formation of crystals and crystal hydrates of salt. On the crystal front there is an increased convection in the liquid, which is caused by the solutal Marangoni flow [29]. The effect of the thermal Marangoni number on convection inside a thin layer of liquid is described in [30, 31].

One of the objectives of the present work is to investigate the behavior of the salt solution when the liquid height decreases by an order of magnitude, which leads to a change in the role of the conductive and convective heat transfer in the layer.

Measuring method

The experiments were carried out at relative air humidity of 30-35%, ambient air temperature of 23 °C, and ambient air pressure of 1 bar. A detailed description of the experimental setup is presented in [19]. The aqueous salt solution was placed on a horizontal heated wall. The working section was made of titanium alloy with diameter $d = 70$ mm. The height of the working section was 50 mm. The measurement of external humidity and ambient temperature has shown no change in time. The initial height of the salt solution for all experiments was the same and equal to 3 mm. Aqueous solutions of salts: LiBr, CaCl₂, LiCl, NaCl, CsCl, BaCl₂, and MgCl₂ were used in the experiments. Thermocouples for wall temperature measurement were located near the wall surface (0.5 mm from the surface). The wall temperature T_w was kept constant in an automatic mode with accuracy within ± 0.5 °C. The interfacial temperature of liquid was determined with the help of thermal imager NEC R500 (resolution of infrared camera was 640×512 pixels). A change in salt concentration did not affect the temperature measurements. The value of initial mass concentrations of salt in aqueous salt solutions (C_{01}) was determined using the densimeters. Current salt concentrations C_{1i} of the aqueous salt solutions were determined by a weight method. The setup was placed on the high-precision balance. The increase in salt concentration leads to the change of the equilibrium partial vapor pressure, p_s , at the interface as well [1]. At the known equilibrium values of temperature, T_s , and equilibrium vapor concentration, C_s , the equilibrium vapor density, ρ_s , is uniquely determined by the equilibrium curves [1, 25-27]. The maximum error of evaporation rate was 10-12 % for large times with low evaporation rate. The experimental study of evaporation rates was conducted before the occurrence of crystallization.

Non-isothermal evaporation and heat transfer of aqueous salt solution layers

Experimental data on evaporation rate J [$\text{kgm}^{-2}\text{s}^{-1}$] are shown in fig. 1. The graphs show intervals of measurement errors. Curves 1-7 represent evaporation rates for different

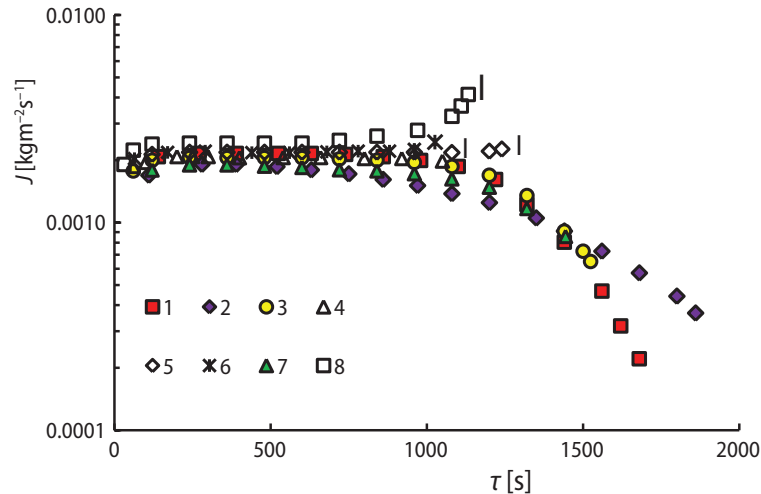


Figure 1. Evaporation rate J [$\text{kgm}^{-2}\text{s}^{-1}$] of aqueous salt solutions (initial salt concentration $C_{01} = 10\%$, $T_w = 78\text{ }^\circ\text{C}$, 1 – LiBr, 2 – LiCl, 3 – CaCl_2 , 4 – NaCl, 5 – CsCl, 6 – BaCl_2 , 7 – MgCl_2 , 8 – H_2O (I is the interval of measurement errors))

salt solutions. For all salt solutions, the initial salt concentration was the same ($C_{01} = 10\%$). Curve 8 corresponds to the evaporation of the distillate. The following important differences between evaporation curves may be noted. The evaporation rate of salt solutions of CaCl_2 , LiCl, LiBr, and MgCl_2 decreases continuously with time. The evaporation rate for water and for salt solutions of CsCl, NaCl, BaCl_2 is quasi constant for the most part of the evaporation time. Different behavior of salts may be explained by different behavior of equilibrium curves. If for water the point on the equilibrium curve is uniquely determined by two parameters $p_s = f(T_s)$, then for salt solutions, the partial pressure, p_s , of water vapor depends on the equilibrium temperature, T_s , and the equilibrium salt concentration, C_s , $p_s = f(T_s, C_s)$ [1]. Since the external humidity during the experiment remains almost constant (it is continuously measured by the humidity meter), the change in p_s will lead to a change in the evaporation rate j (kg/s) in accordance with [32-34]:

$$j \sim D_g(\rho_s + \rho_0) \ln(1 + B_M) \sim p_{vs} \quad \text{if} \quad \rho_s \gg \rho_0 \quad (1)$$

where the equilibrium pressure of steam, p_s , may be expressed through density (vapor concentration, ρ_s) using Mendeleev-Clapeyron equation (ρ_s is the density of water vapor at the interface, D_g is the vapor diffusion coefficient in air, and B_M is the Spalding mass number) [32].

In accordance with the equilibrium curves, an increase in the salt concentration, C_s , leads to a drop in p_s [1, 25-27]. The behavior of equilibrium curves and p_s varies significantly for different salt solutions. As one can see from fig. 1, for both water and all studied salt solutions, there is a slight change in J at time interval $t = 30\text{-}700$ seconds. At $t > 800$ seconds, the evaporation rate for the water layer increases, since a decrease in the layer thickness leads to an increase in T_s and, accordingly, to an increase in the equilibrium partial vapor pressure near the free surface of the liquid. At $t > 800$ seconds, the evaporation rate for the aqueous solutions of LiBr, LiCl, MgCl_2 , and CaCl_2 substantially decreases. For these salts, the growth of salt concentration, C_s , leads to a significant drop of p_s .

Aqueous solutions of NaCl, CsCl, and BaCl₂, salts show a slight increase in J near the crystallization region. For these salts p_s decreases weakly with a substantial increase in the current concentration of salt. It is important to note that the behavior of salts in fig. 1 corresponds to high temperatures of the solution. An essential decrease in T_w temperature can lead to a different evaporation pattern according to the parameters of the equilibrium curves.

The lowest rate of evaporation (before crystallization) for all investigated salts is specific for the LiBr salt. This salt is most often used in absorption heat pumps. The lowest evaporation rate uniquely corresponds to the highest absorption activity in the absorber of the heat pump. High absorption rates noticeably increase the solution temperature due to phase transition and high efficiency of the heat pump. Solubility of LiBr and CsCl salts is high, that allows achieving salt concentrations above 60%. The LiBr salt is applicable in heat pumps for the reasons mentioned above. The aqueous salt solution CsCl-water evaporates very quickly at high concentrations of salt, and therefore will have a very low absorption rate and a very low degree of solution heating in the absorber. Therefore, this salt is not suitable for heat pumps.

The equation of the heat balance for the free surface of a liquid has the form:

$$q_w = \lambda_w \left(\frac{dT}{dy} \right) \Big|_{y=0} = \alpha_1 (T_w - T_s) = q_e, \quad q_e = rJ + \alpha_g (T_s - T_0) + q_r \quad (2)$$

where $q_w = \lambda_w (dT/dy)_{y=0}$ is the heat flux density of the wall, $q = \alpha_1 (T_w - T_s)$ – the heat flux density of the liquid layer, $q_e = rJ$ ($J = \Delta m / F \Delta t$) – the heat flux density due to evaporation, $q_c = \alpha_g (T_s - T_0)$ – the heat flux from gas convection, and q_r – the heat removed from the liquid due to radiation, m – the liquid mass, λ_w – the thermal conductivity of metallic wall, y – the transverse co-ordinate to the wall ($y = 0$ corresponds to the surface of the wall), F – the area of the interface, t – the time, r – the latent heat of evaporation (latent heat of evaporation for aqueous salt solution consists of two heats: the heat of water evaporation and the heat of dilution due to changes in the concentration of salt), α_g – the heat transfer coefficient for steam-gas mixture, resulting from free gas convection over the surface of the heated liquid, and T_0 – the temperature away from the wall. The radiation flux was determined by the expression $q_r = \varepsilon \sigma (T_s^4 - T_0^4)$ [35], where ε is the coefficient of thermal radiation for the fluid, σ – the Stefan-Boltzmann constant. The heat transfer coefficient α_1 for water and for the salt solutions was determined by expression:

$$\alpha_{ii} \approx \frac{q_\Sigma}{\Delta T_i} \quad (3)$$

where $\Delta T_i = T_{wi} - T_{si}$ is the temperature difference near the surface of the wall, T_{wi} – the current average wall temperature, and T_{si} – the current average temperature of the free surface (liquid-gas). The heat transfer coefficient for gas α_g was determined in accordance with [35] by the expression $Nu = \alpha_g R / \lambda_g = 0.54 Ra^{0.25}$, $Ra = g \beta \Delta T_s (R)^3 / \nu a$, where Nu and Ra are the Nusselt and Rayleigh numbers, λ_g – the thermal conductivity of gas, β – the coefficient of thermal expansion, g – the gravity acceleration, and R is the characteristic scale (the radius of the cylindrical heater).

For water and all salt solutions, the condition of heat balance was performed in accordance with eq. (2) for the most part of evaporation time. The difference $\Delta_1 = (q_w - q_\Sigma) 100\% / q_w$ did not exceed 3-5%. In addition, at small and medium times the impact of gas convection and heat radiation is negligible compared to the heat of vaporization. Therefore, the error in determining the convective component had almost no effect on thermal balance performance and accuracy of determining α_1 . At large times, when the heat transfer coefficient significantly

changed over time, the maximum value of Δ_1 reached 10-15%. The growth of Δ_1 was due to the increase of non-stationarity at large times ($dT_w/dt \neq 0$). The upper surface temperature was measured by the thermal imager. The wall temperature was measured by thermocouples. The maximal measurement error α_1 was within 15-17%.

Experimental data on the changes in the ratio of heat transfer coefficients $\alpha_{(water)}/\alpha_{(salt)}$ over time are shown in fig. 2, where $\alpha_{(water)}$ corresponds to heat transfer coefficient for the water layer, and $\alpha_{(salt)}$ corresponds to the water-slat solution.

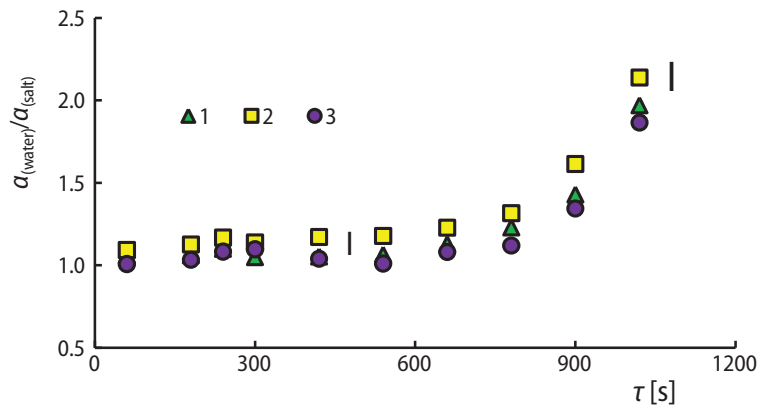


Figure 2. Ratio of heat transfer coefficients $\alpha_{(water)}/\alpha_{(salt)}$ over time ($C_{01} = 10\%$; $T_w = 78$ °C, I is the interval of measurement errors): 1 – LiBr, 2 – CaCl₂, 3 – LiCl

For most of the evaporation time, the heat transfer for water is only slightly greater than α_1 for salts ($\alpha_{(water)}/\alpha_{(salt)} \approx 1$). For $t > 900$ seconds, the coefficient $\alpha_{(water)}$ is much higher than $\alpha_{(salt)}$, which is due to the different height of the liquid h for water and salt solution, as well as to the viscosity of the liquid. For the final stage of evaporation of the water layer, the height, h , becomes less than 0.3-0.4 mm. For such a thin layer, convection is practically suppressed, and heat transfer is determined only by the thermal conductivity $\alpha_{(water)} \approx \lambda/h$. Thus, high heat transfer for water is associated with a small value of h . At $t = 900$ seconds, the height of the salt layer is 3-4 times higher than that of water. It would seem that the salt should show a more intense heat transfer due to free convection (effect of the thermal (Ma_T) and the solutal Marangoni number (Ma_C); $Ma_T = (\Delta T_s h / \mu a)(d\sigma/dT_s)$, where σ is the surface tension of the liquid, μ – the viscosity in the liquid, a – the liquid thermal diffusivity and $Ma_C = (\Delta C_s h / \mu D)(d\sigma/dC_s)$, where ΔC_s is the difference in the salt concentration at the liquid interface, and D – the diffusion coefficient in the aqueous salt solution). In fact, the ratio $\alpha_{(water)}/\alpha_{(salt)} \approx 1.9-2.1$ ($t = 1000$ seconds). For the specified time interval, there is a high concentration of salt and the viscosity of the salt solution is 2-3 times higher than the viscosity of water. Thus, the high viscosity of the solution leads to a significant suppression of convection and heat transfer coefficient.

At $h = 2-3$ mm ($t = 30-100$ seconds), the temperature gradient on the liquid surface $\Delta T_s = 0.4-0.6$ °C, $Ra = 200$, $Ma_T = 3800$. For the time $t = 1050$ seconds ($h = 0.2$ mm, $\Delta T_s = 0.1$ °C), $Ra = 0.5$ and $Ma_T = 50$. Thus, at small times for $h = 2-3$ mm, the Ma_T number exceeds the critical value of 1000-2000, at which the free-convective motion of the liquid occurs [35]. For the evaporation stage at time $t = 1000-1100$ seconds, the values of Ra and Ma_T are much lower than the specified critical value of 2000, and therefore the heat transfer in the layer is determined mostly by conductive heat transfer.

Heat transfer coefficient in fig. 2 not quite clearly reflects the role of convection. It is more convenient to analyze free convection in a liquid considering the graph of change in the Nusselt number ($Nu = \alpha_1 h / \lambda_1$). The Nusselt number characterizes the ratio of heat transfer due to convection to heat transfer due to thermal conductivity.

Figure 3 shows changes in the ratio of Nusselt numbers $A = Nu_{(salt)} / Nu_{(water)}$ with time. Parameter A compares the role of convection for salt solution and water for each time moment τ . The ratio $Nu_{(salt)} / Nu_{(water)} > 1$ for $t > 60$ seconds. As time increases, parameter A grows and has a higher value for LiBr and $CaCl_2$ than for LiCl. The excess of convection for a salt solution ($Nu_{(salt)}$) over that for water ($Nu_{(water)}$) is associated with a large difference in heights, h . Since the evaporation rate for water is higher than for the salt solution, the height of the solution will be, on the contrary, higher than for the water layer. The ratio of heights $h_{(salt)} / h_{(water)}$ increases over time. More intensive convection (Nu number) for salt solutions does not mean that the heat transfer should be higher.

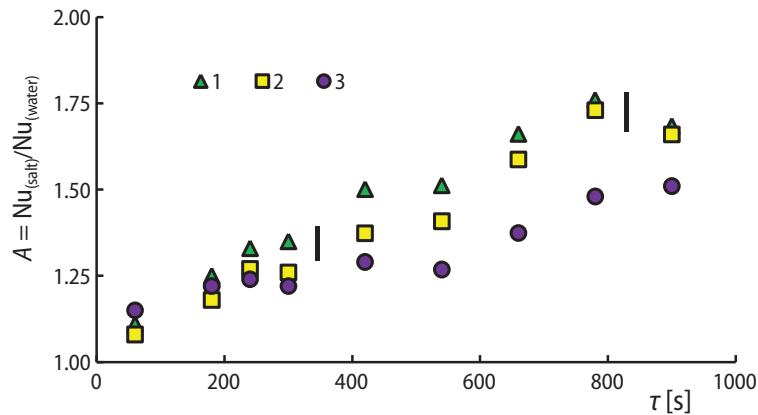


Figure 3. $A = Nu_{(salt)} / Nu_{(water)}$ over time ($C_{01} = 10\%$; $T_w = 78^\circ C$):
1 – LiBr, 2 – $CaCl_2$, 3 – LiCl

From fig. 2 it can be seen that for the final stage of evaporation, α_1 for water significantly exceeds the heat transfer coefficient for salt. Thus, to estimate the heat transfer and the Nusselt number, several parameters must be taken into account simultaneously: the height of the liquid layer, the contribution of free convection to heat transfer (the circulation motion of the liquid inside the layer under the action of thermocapillary and thermogravitation convection), and the contribution of thermal conductivity (the change in molecular thermal conductivity over time due to the increase in salt concentration). These parameters are interrelated and affect each other. For example, due to water evaporation, the salt concentration and the dynamic viscosity, μ , increase and the layer height, h , decreases. As a result, the convection velocity in the liquid, U_c , decreases since $U_c \sim h/\mu$ [36]. In addition to these parameters, convection in the gas also has an important effect on the evaporation rate [37]. This influence is determined by the Rayleigh number for the gas phase and depends on the radius of the layer R and the temperature difference $\Delta T_{s1} = T_s - T_0$, where T_0 is the temperature of the outside air. In the present experiments, this effect is not investigated ($R = \text{constant}$, ΔT_{s1} also changed slightly and insignificantly influenced the change in the Rayleigh number).

Conclusions

Evaporation of the layers of aqueous salt solutions has been studied experimentally. Experimental data are compared with evaporation of the water layer.

The behavior of the evaporation rate, J , differs significantly for different water-salt solutions. Due to the increase in salt concentration over time, the evaporation rate of salt solutions LiBr-water, CaCl₂-water, LiCl-water, and MgCl₂-water decreases several times. Evaporation rates for solutions NaCl-water, CsCl-water, and BaCl₂-water slightly changes over time. The different behavior of salts is due to different values of the equilibrium partial vapor pressure near the free surface of the liquid for different types of salts.

When the water layer and the salt solution evaporate (initial salt concentration $C_{01} = 10\%$), the heat transfer coefficient is constant over a long period of time and increases significantly in the final stage of evaporation due to the multiple decrease in the thickness of the liquid layer. For $t > 900$ seconds, the heat transfer coefficient α for water significantly exceeds α for the salt solution, which is due to the fact that the height of the water layer becomes several times less than the height of the salt solution.

Parameter $A = \text{Nu}_{(\text{salt})}/\text{Nu}_{(\text{water})}$ is greater than unity and increases with time. The effect of convection on heat transfer varies with time and depends on the current salt concentration, dynamic viscosity, thermal conductivity, and solution layer height, which must be considered in the simulation.

Acknowledgment

The experimental studies were carried out within the framework of the state assignment for the IT SB RAS.

Nomenclature

a	– thermal diffusivity
C	– mass concentration
D	– diffusion coefficient
d	– diameter, [mm]
F	– area of layer
g	– gravitational acceleration
h	– layer height
J	– evaporation rate
j	– evaporation rate
Ma_C	– solutal Marangoni number, $[= (\Delta C_s h / \mu D)(d\sigma/dC_s)]$, [–]
Ma_T	– thermal Marangoni number, $[= (\Delta T_s h / \mu \alpha)(d\sigma/dT_s)]$, [–]
m	– mass
Nu	– Nusselt number, $(= \alpha_l h / \lambda_l, \text{ or } = \alpha_g R / \lambda_g)$, [–]
q	– heat flux density
R	– layer radius
Ra	– Rayleigh number, $[= g\beta\Delta T_s(R)^3/v\alpha]$, [–]
r	– latent evaporation heat
T	– temperature
U	– velocity of liquid
y	– co-ordinate

Greek symbols

α	– heat transfer coefficient
β	– thermal expansion coefficient
λ	– thermal conductivity
μ	– dynamic viscosity
ν	– kinematic viscosity
ρ	– density
σ	– Stefan-Boltzmann constant
σ	– surface tension
τ	– time

Subscripts

0	– initial value, ($t = 0$)
0	– a parameter value away from the wall
1	– for salt concentration
c	– convection
e	– evaporation
g	– gas
i	– current value
l	– liquid
r	– radiation
s	– droplet free surface
w	– wall
Σ	– the sum of several factors

References

- [1] Nakoryakov, V. E., Grigoryeva, N. I., *Nonisothermal absorption in thermotransformers*, Nauka, Novosibirsk, Russia, 2010
- [2] Lengyel, P., Morvay, S., *Chemie und Technologie der Zellstoffherstellung*, Akadémiai Kiadó, Budapest, 1973
- [3] Nakoryakov, V. E., *et al.*, Heat and Mass Transfer Intensification at Steam Absorption by Surfactant Additives, *Int. J. Heat and Mass Transfer*, 51 (2008), 21-22, pp. 5175-5181
- [4] Nakoryakov, V. E., *et al.*, Heat and Mass Transfer in the Entrance Region of the Falling Film: Absorption, Desorption, Condensation and Evaporation, *Int. J. Heat Mass Transfer*, 54 (2011), 21-22, pp. 4485-4490
- [5] Nakoryakov, V. E., *et al.*, Heat and Mass Transfer in the Liquid Film on a Vertical Wall in Roll-Wave Regime, *Int. J. Heat Mass Transfer*, 55 (2012), 23-24, pp. 6514-6518
- [6] Ajaev, V. S., *et al.*, Application of Floquet Theory to the Stability of Liquid Films on Structured Surfaces, *Physics of Fluids*, 25 (2013), 12, 122102
- [7] Burelbach, J. P., *et al.*, Steady Thermocapillary Flows of Thin Liquid Layers, II. Experiment, *Phys. Fluids A*, 2 (1990), 3, 322
- [8] Oron, A., *et al.*, Long-Scale Evolution of Thin Liquid Films, *Rev. Mod. Phys.*, 69 (1997), 3, pp. 931-980
- [9] Misyura, S. Y., The Influence of Convection on Heat Transfer in a Water Layer on a Heated Structured Wall, *International Communications in Heat and Mass Transfer*, 102 (2019), Mar., pp. 14-21
- [10] Zheng, Y., *et al.*, Experimental Study of Falling Film Evaporation Heat Transfer on Superhydrophilic Horizontal-Tubes at Low Spray Density, *Applied Thermal Engineering*, 111 (2017), Jan., pp. 1548-1556
- [11] Misyura, S. Ya., Non-Isothermal Evaporation of Salt Solutions on a Microstructured Surface, *Nanoscale and Microscale Thermophysical Engineering*, 22 (2018), 3, pp. 213-229
- [12] Wunder, F., *et al.*, Numerical Simulation of Heat Transfer in a Horizontal Falling Film Evaporator of Multiple-Effect Distillation, *Desalination*, 401 (2017), Jan., pp. 206-229
- [13] Xu, L., *et al.*, Heat-Transfer Film Coefficients of Falling Film Horizontal Tube Evaporators, *Desalination*, 166 (2004), Aug., pp. 223-230
- [14] Meyer, T., Improvement of the Exact Analytical Solutions for Combined Heat and Mass Transfer Problems Obtained with the Fourier Method, *Int. J. Refrigeration*, 43 (2014), July, pp. 133-142
- [15] Grossman, G., Simultaneous Heat and Mass Transfer in Film Absorption under Laminar Flow, *Int. J. Heat and Mass Transfer*, 26 (1983), 3, pp. 357-371
- [16] Meyer, T., Ziegler, F., Analytical Solution for Combined Heat and Mass Transfer in Laminar Falling Film Absorption Using First Type Boundary Conditions at the Interface, *Int. J. Heat Mass Transfer*, 73 (2014), June, pp. 141-151
- [17] Misyura, S. Y., Evaporation and Heat Transfer of a Sessile Drop of Aqueous Salt Solution on Heated Wall, *Int. J. Heat and Mass Transfer*, 116 (2018), Jan., pp. 667-674
- [18] Nakoryakov, V. E., *et al.*, Nucleate Boiling in Pure-Water and Salt-Water Droplets, *Doklady Physics*, 59 (2014), Nov., pp. 441-445
- [19] Nakoryakov, V. E., *et al.*, Nonisothermal Desorption of Droplets of Complex Composition, *Thermal Science*, 16 (2012), 4, pp. 997-1004
- [20] Voitkov, I. S., *et al.*, Temperature of Gases in Trace of Water Droplets During Their Motion in a Flame, *Thermal Science*, 22 (2018), 1A, pp. 335-346
- [21] Misyura, S. Y., *et al.*, Temperature and Velocity Fields Inside a Hanging Droplet of a Salt Solution at Its Streamlining by a High-Temperature Air Flow, *Int. J. Heat Mass Transfer*, 129 (2019), Feb., pp. 367-379
- [22] Volkov, R. S., *et al.*, Fire Extinction of Forest Fuels by Droplets and Water Film, *Thermal Science*, 22 (2018), 1A, pp. 347-358
- [23] Misyura, S. Y., Free Solution Convection at Non-Isothermal Evaporation of Aqueous Salt Solution on a Micro-Structured Wall, *Nanoscale and Microscale Thermophysical Engineering*, 23 (2019), 1, pp. 48-66
- [24] Misyura, S. Y., Morozov, V. S., Droplet Evaporation on a Heated Structured Wall, *Thermal Science*, 23 (2019), 2A, pp. 673-681
- [25] Conde, M. R., Properties of Aqueous Solution of Lithium and Calcium Chlorides: Formulations for Use in Air Conditioning Equipment Design, *Int. J. of Thermal Sciences*, 43 (2004), 4, pp. 367-382
- [26] Ogawa, K., Thermodynamic Properties of Aqueous Solution of Lithium Bromide, Measurement of Specific Heat at Atmospheric Pressure, *Refrigeration (Japan)*, 55 (1980), 630, pp. 347-351
- [27] Lower, H., *Thermodynamische und Physikalische Eigenschaften der Wassrigen Lithiumbromid-Lösung*, Dissertation, T. H., F. f. Maschinenw, Karlsruhe, Germany, 1960

- [28] Ibarra-Bahena, J., *et al.*, Experimental Assessment of a Hydrophobic Membrane-Based Desorber/Condenser with H₂O/LiBr Mixture for Absorption Systems, *Experimental Thermal and Fluid Science*, 88 (2017), Nov., pp. 145-159
- [29] Kuznetsov G. V., *et al.*, Marangoni Flow and Free Convection During Crystallization of a Salt Solution Droplet, *Colloids and Surfaces A: Physicochemical and Engineering Aspects*, 572 (2019), July, pp. 37-46
- [30] Hu, H., Larson, R. G., Analysis of the Effects of Marangoni Stresses on the Microflow in an Evaporating Sessile Droplet, *Langmuir*, 21 (2005), 9, pp. 3972-3980
- [31] Hu, H., Larson, R. G., Marangoni Effect Reverses Coffee-Ring Depositions, *J. Phys. Chem. B.*, 110 (2006), 14, pp. 7090-7094
- [32] Spalding, D. B., The Combustion of Liquid Fuels, *Proc. Combust. Inst.*, 4 (1953), 1, pp. 847-864
- [33] Carle, F., *et al.*, Contribution of Convective Transport to Evaporation of Sessile Droplets: Empirical Model, *Int. J. Therm. Sci.*, 101 (2016), Mar., pp. 35-47
- [34] Kelly-Zion, P. L., *et al.*, Evaporation of Sessile Drops under Combined Diffusion and Natural Convection, *Colloid Surf. A*, 381 (2011), 1-3, pp. 31-36
- [35] Kutateladze, S. S., *Fundamentals of Heat Transfer Theory*, Atomizdat, Moscow, 1979
- [36] Volkov, R. S., *et al.*, The Influence of Key Factors on the Heat and Mass Transfer of a Sessile Droplet, *Experimental Thermal and Fluid Science*, 99 (2018), Dec., pp. 59-70
- [37] Misyura, S. Y., Effect of Various Key Factors on the Law of Droplet Evaporation on the Heated Horizontal Wall, *Chemical Engineering Research and Design*, 129 (2018), Jan., pp. 306-313